A meanfield theory of grain boundary segregation

William L. Alba and K. Birgitta Whaley

Citation: J. Chem. Phys. **95**, 4427 (1991); doi: 10.1063/1.461766
View online: http://dx.doi.org/10.1063/1.461766
View Table of Contents: http://jcp.aip.org/resource/1/JCPSA6/v95/i6
Published by the American Institute of Physics.

A mean-field theory of grain boundary segregation

William L. Alba and K. Birgitta Whaley
Department of Chemistry, University of California, Berkeley, California 94720

(Received 25 January 1991; accepted 7 June 1991)

This paper presents a mean-field solution for a one-dimensional spin Hamiltonian in the presence of spatially varying interactions and external field. In a binary alloy, such inhomogeneous interactions appear in the presence of a grain boundary. We derive the model and place it in the context of previous theories. We show how our theory is a natural extension of traditional segregation isotherm models, with the advantages that much finer detail can be observed and that no assumption is required about the grain boundary binding energy. Solving the model requires finding the global minimum of a function of several hundred variables and yields detailed concentration profiles in the presence of spatially inhomogeneous and long-range interactions. We apply the theory to the system of copper with bismuth impurities and observe on an atomic scale how the extent of segregation varies with temperature. The results predict that with lower temperature the impurity concentration in a given layer increases, the segregant peak broadens, and ordering can occur within the boundary. The results also indicate that the presence of segregation at the grain boundary can serve as a nucleus for order–disorder phase transitions in the bulk.

I. INTRODUCTION

The segregation of impurities to grain boundaries affects numerous important properties of metals and alloys, such as fracturing, embrittlement, and stress corrosion.[1] Considerable experimental effort has been devoted to the characterization of segregation profiles and of segregation-induced boundary structural changes. While these techniques can in principle resolve chemical species on the atomic scale,[2] practical limitations have so far hampered experimental study at this level of detail. The lateral distribution of segregant species in the boundary region and the effect of this arrangement on metallurgical properties remain experimentally unknown.

Theories of segregation have also neglected structural and chemical effects at the interatomic level. Segregation isotherms,[3] the interfacial analog of gas–surface adsorption isotherms, possess only limited explanatory value, because they fail to provide structural detail on the atomic level, and they lack predictive value, because their parameters are empirically fit to a specific experiment. *Ab initio* calculations to determine these binding parameters have involved only one or a small number of segregant atoms at the boundary. These substitutional insertion calculations neglect the importance of segregant atoms affecting each other and are valid only in the limit of infinite dilution of the impurity in the bulk.[4]

Both recent experiments[5] and theory[6] suggest the possibility of quasi-two-dimensional phase transitions in the boundary layer accompanying equilibrium segregation, analogous to adsorbate ordering transitions in surface segregation and in gas–surface adsorption.[7] The experimental evidence for such transitions is inconclusive and further study will require finer chemical resolution. At the same time, it is imperative to develop a microscopic theory of segregation, in order to investigate the lateral segregant distribution at an atomic level, to understand the role of bulk and boundary structure and atomic interactions, and to discern the relation of boundary to bulk phase transitions.

As the first stage in such a microscopic approach, we present a mean-field theory which predicts the equilibrium structure of the segregant near a high-angle tilt boundary as a function of distance, on an atomic scale. (While a grain boundary is, strictly speaking, a nonequilibrium structure, it exists on a time scale long enough to be considered equilibrium from the point of view of substitutional ordering.) This model indicates that the grain-boundary segregant can order, and that the width of the segregant distribution can change with temperature. Most significantly, results from this model suggest that ordering of the grain boundary segregant can induce phase transitions to occur in the bulk. The theory requires only knowledge of the geometry of the bicrystal and of the finite-range interactions between different sites. This mean-field approach serves as a complement to computer simulation[8,9] and to experimental studies of grain boundary segregation.

Section II describes the parameters of a model grain boundary system, maps the binary alloy to a spin system, and places the model in the context of existing segregation isotherm models. Section III presents the method of solution for the model, which is equivalent to finding the global minimum of a function of several hundred variables. In Sec. IV we apply the method to a specific example, the [210] $\Sigma = 5$ copper/bismuth system, and in Sec. V we state our conclusions.

II. DERIVATION AND DISCUSSION OF THE MODEL

A. Isomorphism of binary alloy with spin model

In this paper, we focus on high-angle symmetrical tilt boundaries, whose structure is well-represented by the coincidence site lattice (CSL) model.[10] An example is shown in Fig. 1. The fixed sites of the bicrystal lattice are populated with either the bulk (solvent) component A or the impurity (solute) component B. These atoms interact pairwise within some finite range, R. The Hamiltonian for this generalized binary alloy is

 0021-9606/91/184427-12$03.00

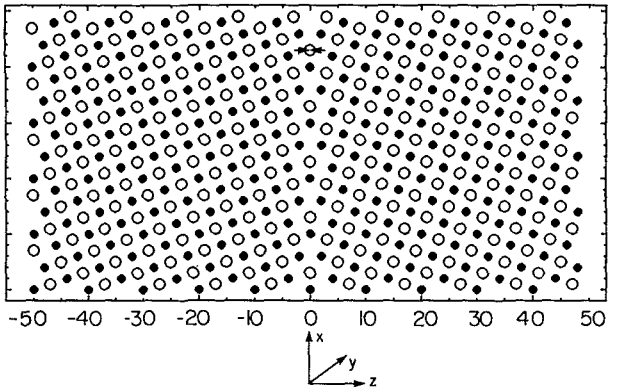

FIG. 1. A sample bicrystal computational cell. The structure is a [210] $\Sigma = 5$ grain boundary in an fcc crystal. Each circle represents a site, populated by bismuth or copper in the binary system studied here. Two planes are shown: the small dark circles lie 1.807 Å below the large open circles. These two atomic planes repeat along the z direction. At the central grain boundary plane, two sites which would have been 1.14 Å apart are eliminated and replaced by one site at the central layer, as indicated by the arrows.

$$\mathscr{H} = 1/2 \sum_i \sum_j (\phi_{ij}^{A-A} c_i^A c_j^A + 2\phi_{ij}^{A-B} c_i^A c_j^B + \phi_{ij}^{B-B} c_i^B c_j^B) + \sum_i (c_i^A \mu^A + c_i^B \mu^B), \quad (1)$$

where ϕ_{ij}^{X-Y} represents the potential between species X at site i and species Y at site j (in this paper, we will assume that ϕ depends only on the distance between the sites, but this is not essential), μ^X represents the chemical potential of species X, which is uniform over the bicrystal lattice at thermodynamic equilibrium, and c_i^X represents the occupation number of species X at site i. The latter is either zero or unity at each site, so that c^A is 1 and c^B is 0 when species A occupies site i, and $c^A = 1 - c^B$.

The Hamiltonian for a general Ising model is

$$\mathscr{H} = -1/2 \sum_i \sum_j J_{ij} s_i s_j - \sum_i H_i s_i + C, \quad (2)$$

where J_{ij} is the spin–spin coupling between the spins at sites i and j (with J_{ii} defined to be zero), H_i is an external magnetic field which acts on the spin at site i, C is a constant energy term, and the spin variable s_i on site i takes on values of ± 1. In contrast to Eq. (1), which is grand canonical because the relative number of bismuth and copper atoms is allowed to vary, Eq. (2) is in a canonical representation, since the number of spins is constant. By mapping the concentration variables onto the spin variables,

$$c_i^A = 1/2(1 + s_i),$$
$$c_i^B = 1/2(1 - s_i), \quad (3)$$

we obtain the usual isomorphism between these two Hamiltonia, with

$$J_{ij} = 1/2[\phi_{ij}^{A-B} - 1/2(\phi_{ij}^{A-A} + \phi_{ij}^{B-B})], \quad (4)$$

$$H_i = 1/4 \sum_j (\phi_{ij}^{B-B} - \phi_{ij}^{A-A}) + 1/2(\mu^B - \mu^A), \quad (5)$$

$$C = 1/8 \sum_{i \neq j} (\phi_{ij}^{A-A} + \phi_{ij}^{A-B} + \phi_{ij}^{B-B}) + 1/2(\mu^B - \mu^A). \quad (6)$$

Because the grand-canonical binary alloy and the canonical Ising model are equivalent, throughout this paper we refer interchangeably to both of these models, interconverting with the equalities in Eqs. (4)–(6). Note that due to the translational symmetry breaking introduced by the grain boundary, both parameters J_{ij} and H_i depend on the z coordinate, the perpendicular distance from the grain boundary (Fig. 1).

The magnetic field H_i, which is invariant within a given plane parallel to the grain boundary, contains a sum over all interactions within range of site i. Since a site near the grain boundary interacts with other sites at distances which do not occur in the bulk (Fig. 1), H_i is also a function of distance from the grain boundary. However, inside an atomic layer, all sites are crystallographically equivalent, so H_i is constant in the x and y directions. The relative magnitudes of $(\phi_{ij}^{A-A} + \phi_{ij}^{B-B})$ and ϕ_{ij}^{A-B}, as well as the chemical potentials μ^A and μ^B, determine the overall concentration ratio of A to B.

In the copper/bismuth example given in Sec. IV, the magnetic field H_i is always negative and this inhibits the appearance of spin + 1, i.e., of bismuth. However, since H_i will be shown to be least unfavorable for bismuth in the grain boundary region, if any bismuth exists in the system, it will preferentially occupy the sites near the grain boundary at equilibrium. Therefore, the conversion from the binary alloy model to the spin model simplifies mathematical manipulations, places our theory in a more general form, and immediately yields the magnetic field, the inhomogeneity of which indicates the occurrence of segregation.

B. Mean-field approximation

At this point we introduce the mean-field approximation and assume that all the crystallographically equivalent sites in a given layer n perpendicular to the grain boundary possess an average impurity concentration C_n^A (capital letters will denote mean-field variables, and lower case letters will denote site variables). Equivalently, in Ising spin terminology, averaging over the spins in the nth atomic plane gives the mean-field spin variable, or magnetization, $S_n = 2C_n^A - 1$. Note that because spins s_i within a given layer interact with spins in the same layer, each mean-field spin S_n is coupled to itself as well as to neighboring layers (i.e., $J_{nn} \neq 0$). Averaging the interactions over the two spatial dimensions parallel to the grain boundary produces concentration profiles, which depict the average concentration in an atomic plane n as a function of the perpendicular distance z of these planes from the center of the grain boundary.

From the Gibbs–Bogoliubov inequality, one can derive the mean-field Gibbs free energy appropriate to Eq. (2),

$$G_{\mathrm{MF}} = -1/2 \sum_n \sum_{n'} \langle J_{nn'} \rangle S_n S_{n'} - \sum_n H_n S_n + kT \sum_n [1/2(1 + S_n) \ln 1/2(1 + S_n) + 1/2(1 - S_n) \ln 1/2(1 - S_n)]. \quad (7)$$

Here $\langle J_{nn'} \rangle$ is the coupling between two layers, defined as

$$\langle J_{nn'} \rangle = \sum_{J_{n'}} J_{i_n j_{n'}}. \tag{8}$$

The summation is restricted, requiring that site i is in the nth layer and each site j is in the n'th layer. Within the bulk, the form of $\langle J_{nn'} \rangle$ is constant and depends only on $|n-n'|$, the distance between the layers. Near the grain boundary, because of the interactions between sites across the boundary, $\langle J_{nn'} \rangle$ becomes asymmetrical. In a coincident site lattice, this first occurs when the grain boundary center is within the potential cutoff distance. H_n is the external applied magnetic field, which is constant except near the grain boundary, where it depends on the layer number n. H_n has the same form as H_i; in the notation of Eq. (8), $H_n = H_{i_n}$, where i is any site in layer n. The last term is the ideal entropy term. For numerical purposes, in a finite-sized system G_{MF} is calculated with periodic boundary conditions, and the number of layers in the system is set to be commensurate with the maximum wavelength of any expected ordered structures.

The Gibbs free energy may be written with the layer–layer interactions expressed in terms of a lattice-difference operator

$$L_n S_n = -\sum_{n'} \langle J_{nn'} \rangle S_{n'} = -\sum_{p=0}^{R/2} d_{2p} \Delta_{n'}^{2p} S_{n'}. \tag{9}$$

The discrete difference operators are defined in the usual manner: $\Delta_n^0 S_n = S_n$, $\Delta_n^2 S_n = S_{n+1} - 2S_n + S_{n-1}$, $\Delta_n^4 S_n = S_{n+2} - 4S_{n+1} + 6S_n - 4S_{n-1} + S_{n-2}$, etc. The coefficients d_{2p} are then linear functions of the layer–layer couplings $J_{nn'}$, where the specific functional form of the coefficients depends on the geometry of the system. The local Gibbs free energy for layer n can now be written,

$$\begin{aligned} G_{\mathrm{MF},n} = {} & 1/2 S_n L_n S_n - H_n S_n \\ & + 1/2 kT\{(1+S_n)\ln[1/2(1+S_n)] \\ & + (1-S_n)\ln[1/2(1-S_n)]\}, \end{aligned} \tag{10}$$

and the total energy is a sum of these individual local energies. The nth element of the gradient of the Gibbs free energy is

$$\frac{\partial G_{\mathrm{MF}}}{\partial S_n} = L_n S_n - H_n + kT \tanh^{-1} S_n \tag{11}$$

and the elements of the Jacobian matrix are

$$\frac{\partial^2 G_{\mathrm{MF}}}{\partial S_n \partial S_{n'}} = \left(L_n + \frac{kT}{1-S_n^2} \right) \delta_{nn'}. \tag{12}$$

Recent interest has focused on finding mean-field phase diagrams for lattice Hamiltonia by finding zeros of the Jacobian [Eq. (12)] to identify second-order phase transitions.[11] In addition to locating the phase transition, we aim to determine the entire mean-field concentration profile over a wide temperature range. This requires finding the set of spins which globally minimize the multidimensional function $G_{\mathrm{MF}}(\{S_n\})$ at each temperature for the spatially inhomogeneous system.[12] Note that although these equations provide only a one-dimensional mean-field concentration profile, the coupling terms do contain all the three-dimensional information, including the inhomogeneity caused by the boundary. Thus we can expect the phase transformation predicted by the one-dimensional mean-field solution to faithfully represent primary features of the three-dimensional system.

C. Relation to segregation isotherms

Before solving for the set of variables which minimize Eq. (8), we will demonstrate that this mean-field theory may be viewed as the finest possible one-dimensional extension of existing segregation isotherm theories.[3] One general derivation of these isotherms divides the bicrystal lattice into two well-defined volumes, a region near the grain-boundary and a bulk-crystal region. Given the impurity concentrations $c_{\mathrm{g.b.}}$ and c_{bulk} in those regions, the Gibbs free energies are written

$$\begin{aligned} G_{\mathrm{g.b.}} = {} & E_{\mathrm{g.b.}} + kT \\ & \times [c_{\mathrm{g.b.}} \ln c_{\mathrm{g.b.}} + (1-c_{\mathrm{g.b.}})\ln(1-c_{\mathrm{g.b.}})], \end{aligned} \tag{13}$$

$$\begin{aligned} G_{\mathrm{bulk}} = {} & E_{\mathrm{bulk}} + kT[c_{\mathrm{bulk}} \ln c_{\mathrm{bulk}} \\ & + (1-c_{\mathrm{bulk}})\ln(1-c_{\mathrm{bulk}})], \end{aligned} \tag{14}$$

where $E_{\mathrm{g.b.}}$ and E_{bulk} represent the internal energy of the grain boundary and of the bulk, respectively. By setting the chemical potentials of the two regions equal to each other, we obtain the general form of a segregation isotherm,

$$\frac{c_{\mathrm{g.b.}}}{1-c_{\mathrm{g.b.}}} = \frac{c_{\mathrm{bulk}}}{1-c_{\mathrm{bulk}}} \exp(-\Delta e/kT). \tag{15}$$

$\Delta e = e_{\mathrm{g.b.}} - e_{\mathrm{bulk}}$ is the change in energy when an impurity atom is transferred from the bulk to the grain boundary $[e_{\mathrm{g.b.(bulk)}} = \partial E_{\mathrm{g.b.(bulk)}}/\partial c_{\mathrm{g.b.(bulk)}}]$. This is often termed the "binding energy." The various isotherm theories differ in the assumptions they make regarding the binding energy. The Langmuir–McLean theory assumes the binding energy is a constant, the Fowler–Guggenheim theory assumes it is a linear function of the grain-boundary impurity concentration, and a recent model by Brokman[6] derives the binding energy as a linear function of both the grain-boundary concentration and the bulk concentration.

These theories suffer from several deficiencies. First, whatever the form of the binding energy function, its coefficients are empirical. Second, the dividing line between the grain boundary region and the bulk region is also arbitrary; our results in Sec. IV show that the thickness of the grain boundary actually varies with temperature. Finally, the resolution of these theories is extremely coarse, since space is divided into only two regions, so that they are all essentially macroscopic Gibbsian segregation descriptions.

Our mean-field theory, while related to these segregation isotherms, overcomes their main deficiencies. As we have seen, the mean-field Gibbs free energy may be written as a sum of local Gibbs free energies of individual layers. Analogous to the way that segregation isotherms divide space into two regions, our model resolves the bicrystal into atomic planes. This finer division permits us to predict variations in concentration on an atomic scale. Both models are also similar because their method of solution can be derived by examining the relevant first derivative of the local Gibbs

free energies. To guarantee stability, in the simple isotherm models, the chemical potentials in the two regions must be equal to each other; in our theory, Eq. (11) must be zero for all n layers.

Unlike the segregation isotherms, however, our division into regions associated with different concentration variables is not arbitrary, but is based on the geometry of the lattice. Furthermore, the energy which drives segregation in our model comes directly from the particle interactions and depends only on the system's geometry. We have already noted how the inhomogeneity of H_n [Eq. (5)] in the Ising representation can give rise to segregation. This magnetic field contains much more detailed information on the differences in local site energies between bulk and boundary regions than a single binding energy. To summarize, unlike segregation isotherms, our model is well-suited for microscopic studies, which require a level of detail that differentiates among energetically inequivalent sites in the grain boundary.

III. NUMERICAL SOLUTION

Finding the global minimum of a spatially inhomogeneous expression like Eq. (8) with several hundred layers is nontrivial. Traditional methods of global optimization, such as simulated annealing[13] and related Monte Carlo methods, are computer intensive and may yield spurious metastable states. Having applied simulated annealing to this problem with only limited success, we found the global minimum in the following manner.

The main difficulties in finding the global minimum of Eq. (8) are that the forms of the layer–layer couplings $J_{nn'}$ and of the magnetic field H_n change as we approach the interface. Therefore, we first find the global minimum of the system in the absence of a grain boundary. We accomplish this in two steps: (i) by finding the wavelength of the sinusoidal or cosinusoidal profile with the lowest Gibbs free energy, and then (ii) fine-tuning the shape of that profile via local minimization. After finding the profile that minimizes the free energy in the bulk, we (iii) input this into a grain boundary system and find the minimum from that starting point using local minimization techniques. Since the boundary introduces a small perturbation compared to the size of the bulk system, it is reasonable to assume that the global minimum of the entire system is obtained by this local minimization. In addition, our knowledge of the bulk global-minimum profile allows us to check the profile at distances far from the grain boundary.

A. Sinusoidal bulk concentration profile

When the number of spin–spin variables determining the d_{2p}'s in Eq. (10) equals 2, one can analytically determine the phase diagram.[11] Under such a scheme, one sets Eqs. (11) and (12) to zero and solves them simultaneously to derive the order wave number q and the transition temperature for those spin–spin interactions. However, these phase diagrams do not give explicit information about the shape of the concentration profile. In addition, in our copper/bismuth example, we have spin–spin interactions to fourth-nearest-neighbor in the bulk, corresponding to mean-field layer–layer interactions to eighth-nearest-neighbors, so we have developed a more general method of solution to solve for the bulk concentration profile.

We begin by assuming that the profile which minimizes G_{MF} can be Fourier decomposed into a sum of sinusoidal and cosinusoidal profiles with amplitude A, order parameter q, and average magnetization $\overline{A}$, i.e.,

$$S_n = A\sin(qn) + \overline{A},$$
$$S_n = A\cos(qn) + \overline{A}. \tag{16}$$

The wave number q is $2\pi/\lambda$, where in practice λ is an integer between 1 and 240, the largest number of planes we have treated. ($\lambda = 1$) gives a flat profile. For brevity we will refer to all states with $\lambda = 1$ as "paramagnetic" regardless of the value of $\overline{A}$ and will not further distinguish true paramagnetism ($\overline{A} = 0$) from metamagnetism ($0 < |\overline{A}| < 1$) or from ferromagnetism ($|\overline{A}| = 1$). ($\lambda = 2$) cosinusoidal waves represent profiles with alternating layers rich and deficient in the impurity, and we will call these antiferromagnetic states. Larger λ's describe phases with longer wavelength order.

Next, we must determine the magnetic field necessary for a given $\overline{A}$, since the average concentration, not the chemical potential, is experimentally controlled and measured. The magnetic field needed to sustain an average magnetization $\overline{A}$ is a function of temperature T, amplitude A, and the wavelength λ of the ordered phase. We find this field by requiring Eq. (11) to be zero for all n, a condition which must be true for any stable or metastable phase. For a sinusoidal phase,

$$H_n = L_n[A\sin(qn) + \overline{A}] + kT\tanh^{-1}[A\sin(qn) + \overline{A}]. \tag{17}$$

While these equations hold true for all n, H_n itself must be uniform over all layers, since it consists of [Eq. (5)] a chemical potential difference (which must be constant over space at equilibrium) and the sum over spin–spin couplings (which is also constant in the bulk, since every layer experiences the same such interactions). Therefore, if we express H as a Fourier sum,

$$H = \frac{a_0}{2} + \sum_{m=1}^{\infty}[a_m\cos(mqn) + b_m\sin(mqn)], \tag{18}$$

we obtain the following stability conditions for a pure sinusoidal profile by comparing the Fourier coefficients.

a_0:

$$-H + d_0\overline{A} + \frac{q}{2\pi}\int_0^{2\pi/q} kT\tanh^{-1}[A\sin(qn) + \overline{A}]\,dn; \tag{19}$$

$a_m\,(m \geqslant 1)$:

$$\frac{q}{\pi}\int_0^{2\pi/q}\{L_n[A\sin(qn) + \overline{A}] + kT\tanh^{-1}[A\sin(qn) + \overline{A}]\}\cos(mqn)\,dn; \tag{20}$$

b_1:

$$\frac{q}{\pi}\int_0^{2\pi/q}\{L_n[A\sin(qn) + \overline{A}] + kT\tanh^{-1}[A\sin(qn) + \overline{A}]\}\sin(qn)\,dn; \tag{21}$$

$b_m (m \geq 2)$:

$$\frac{q}{\pi} \int_0^{2\pi/q} \{L_n [A \sin(qn) + \overline{A}\,] + kT \tanh^{-1}[A \sin(qn) + \overline{A}\,]\} \sin(mqn) dn. \quad (22)$$

Expressions (19)–(22) must be equal to zero for stability of a particular sine concentration profile; similar equations hold for the pure cosinusoidal profile. Since the a_0 term alone determines the field, expression (19) is sufficient to determine H. Note that only the d_0 coefficient survives from the L_n operator.

Expressions (20)–(22) must also be fulfilled to satisfy the stability condition. Applying a discrete-difference operator to $\sin(qn)$ [or $\cos(qn)$] gives the product of $\sin(qn)$ [$\cos(qn)$] with a function which depends only on q and p,

$$\Delta_n^{2p} [\sin(qn)] = f(q,p) \sin(qn). \quad (23)$$

Therefore, for a pure sine wave, expression (20) and the first term in expression (22) are always zero. For a pure cosine wave, expression (21) and (22) and the first term in expression (20) are also analytically zero. A numerical scheme such as Romberg's method[14] is necessary to evaluate the remaining integrals. On performing this calculation, we find that the value of expressions (20)–(22) for each of the pure sine and cosine waves in our copper/bismuth system is *not*, in general, zero. For the reasons discussed in Sec. III B below, this suggests that these amplitude-bounded sinusoidal waves are by themselves insufficient to reconstruct the globally stable phase.

The only remaining variable required to calculate $G_{\rm MF}$ for a given set of layer–layer interactions, temperature, and order parameter q, is the amplitude A. We apply Brent's method[14] to solve for the amplitude that minimizes $G_{\rm MF}(A)$. In order to bracket the minimum properly, the amplitude must lie between zero and that value which would put any layer variable S_n outside of the physical limits $[-1, +1]$. We guarantee this condition by manipulating a transformed variable

$$\tau = \tan \frac{\pi A}{2A_{\max}}, \quad (24)$$

where $A_{\max} = \max(\overline{A} + 1, 1 - \overline{A})$, and then transforming back

$$A = \frac{2}{\pi} A_{\max} |\tan^{-1} \tau| \quad (25)$$

whenever A is needed in the calculation. This transformation stretches the physically allowed range $[0, A_{\max}]$ and maps it onto $[0, \infty]$.

B. Fine-tuning the bulk concentration profile

By calculating $G_{\rm MF}$ for wavelengths ranging from one layer spacing to a physically large number of layers (in our case, 240 layers, or 137.1 Å), for our given temperature T, desired magnetization $\overline{A}$, and layer–layer interactions $\langle J_{nn'} \rangle$, we can find the minimum Gibbs free energy, the corresponding wavelength, and amplitude for the most stable sinusoidal concentration profile, and the magnetic field necessary to sustain $\overline{A}$. We need to verify these values for the following reasons.

First, we have determined what magnetic field H is necessary for a given magnetization $\overline{A}$ and a sinusoidal profile with amplitude $|A| \leq 1$, but we cannot guarantee that, given H, the most stable phase will have $\overline{A}$ when the layer concentrations are allowed to vary independently. Indeed, in Monte Carlo simulations on this copper/bismuth system[9] where we allowed the concentrations to vary freely, we observed that at low temperatures the average magnetization cannot always be brought to a desired value, for any reasonable value of the external field. Second, because we limited the amplitude of the sinusoidal waves so that they never exceed the physical bounds $[-1, +1]$, even though we considered every discrete wavelength in our system, our Fourier decomposition is incomplete. Using such amplitude-bounded sinusoidal waves, for example, one cannot construct a high-amplitude square-wave profile. Therefore, details of the shape of the profile are unavailable by examining sinusoidal waves with restricted amplitudes alone. Finally, since the previous two factors alter the character of the ordered phase, in particular allowing nonsinusoidal profiles, the transition temperature may shift to a different value than predicted from the pure sinusoidal profile.

To account for these additional factors, at each temperature we perform a local minimization on every pure sinusoidal and cosinusoidal profile which displays a nonzero amplitude at any temperature. In the copper/bismuth example, these include the flat paramagnetic ($\lambda = 1$), the antiferromagnetic ($\lambda = 2$), and eight additional profiles. We expect these profiles to encompass the wavelengths of all possible stable phases and also assume that H is correct. Since our process to find a local minimum freely varies S_n for every layer n, the concentration profile will now adjust to change its shape and find the proper $\overline{A}$.

The local minimization procedure to minimize $G_{\rm MF}$ as a function of the set of layer spins S_n is a modified conjugate-gradient method.[14] We again use the stretching transformation Eqs. (24) and (25) to smoothly constrain each layer spin between the physical limits $[-1, +1]$. We apply a more rigorous constraint for convergence than usual by requiring not only that successive iterations have a small relative difference in $G_{\rm MF}$, but also that every element of $\nabla G_{\rm MF}$ with respect to the transformed variable τ_n be small. This additional constraint will be particularly important when we minimize $G_{\rm MF}$ with a grain boundary, since testing only for the constancy of the energy may indicate convergence even if the spin values in a small region near the boundary are in unstable positions. To help accommodate this stricter constraint, we restart the conjugate-gradient search whenever the energy test is fulfilled but our gradient test is not.

C. Concentration profile in the presence of the grain boundary

Having determined the characteristics of the bulk profile which gives the global minimum of the Gibbs free energy, we can now find the lowest-energy phase with a grain boundary in the following manner. We start with those bulk profiles which were the global minima at any of the investigated temperatures and modify the Hamiltonian to contain

the appropriate grain boundary layer–layer and layer–field inhomogeneous interactions. Since the grain boundary represents a physically small perturbation compared to the rest of the bicrystalline lattice, starting with the globally minimized bulk profile and finding the local minimum in the presence of the boundary should yield the globally minimized profile in a system with a grain boundary. In addition, knowing the most stable bulk phase allows us to examine the bulk region surrounding the interface and to judge whether that portion of the profile is reasonable.

This local minimization occurs under the same conditions as that in Sec. II B. In the following section, we describe an application of these inhomogeneous mean-field equations to obtain a segregation profile for the copper/bismuth system as a function of temperature.

IV. EXAMPLE: COPPER/BISMUTH

A. Geometry and potentials

We selected the copper/bismuth system as our model system, because it is a well-known binary system for which simple empirical potentials are available[15] and because the degree of experimentally observed bismuth segregation is quite high.[16] This is also the system studied in the earlier Monte Carlo simulations of Chang, Lee, and Stein.[17] Bismuth is a substitutional impurity in the copper face-centered-cubic crystal, and its segregation causes grain boundary embrittlement of the copper/bismuth alloy.[18]

As mentioned in Sec. II, we are working with high-angle symmetrical tilt boundaries, for which the bicrystal structure is well determined by the CSL model. Since we are primarily interested in analytic characterization of the segregant distribution at this point, the lattice sites are immobile. In this model, shown in Fig. 1, a face-centered-cubic crystal lies on either side of the boundary, with the lattice parameters of bulk copper (nearest-neighbor distance 2.556 Å) and with atoms coincident with the lattice positions of both crystals at the center of the boundary (Fig. 1). We make one modification to the CSL and treat the two atomic sites adjacent to the interface, which would have been 1.14 Å apart and resulted in unrealistically excessive repulsive interactions, as one site at an intermediate distance at the center of the grain boundary.[17]

The tilt angle is $\sim 36.87°$ around the $\langle 100 \rangle$ axis, yielding a reciprocal volumetric density of coincidence sites of $\Sigma = 5$. The grain boundary and the atomic layers parallel to it are [210] planes. The concentration profiles depict the average bismuth concentration in each of these planes, as a function of perpendicular distance from the center of the grain boundary. The geometry of the system determines the form of the function $f(q,p)$ in Eq. (23), and Table I gives these values for our system.

Each lattice site contains a copper (bulk) atom or a bismuth (impurity) atom. The atoms interact pairwise via Morse potentials with the same parameters as those of Chang *et al.*[17] and are truncated at the fourth-nearest-neighbor bulk distance, giving the ϕ's in Eq. (1),

$$\phi(r) = D\{\exp[-2\alpha(r-\beta)] - 2\exp[-\alpha(r-\beta)]\}. \quad (26)$$

TABLE I. $f(q,p)$.[a]

p	$f(q,p)$
0	1
1	$2\cos(q) - 2$
2	$2\cos(2q) - 8\cos(q) + 6$
3	$2\cos(3q) - 12\cos(2q) + 30\cos(q) - 20$
4	$2\cos(4q) - 16\cos(3q) + 56\cos(2q) - 112\cos(q) + 70$
5	$2\cos(5q) - 20\cos(4q) + 90\cos(3q) - 240\cos(2q) + 420\cos(q) - 252$
6	$2\cos(6q) - 24\cos(5q) + 132\cos(4q) - 440\cos(3q) + 990\cos(2q) - 1584\cos(q) + 924$
7	$2\cos(7q) - 28\cos(6q) + 182\cos(5q) - 728\cos(4q) + 2002\cos(3q) - 4004\cos(2q) + 6006\cos(q) - 3432$
8	$2\cos(8q) - 32\cos(7q) + 240\cos(6q) - 1120\cos(5q) + 3640\cos(4q) - 8736\cos(3q) + 16016\cos(2q) - 22880\cos(q) + 12870$

[a] $f(q,p)$ are the coefficients of the lattice difference operators in Eq. (23).

Table II gives values for the parameters D, α, and β for the Cu–Cu, Bi–Bi, and Cu–Bi interactions. The pair potentials are plotted in Fig. 2, where we indicate the normal bulk pair separations (filled circles) and additional pair interactions introduced by the presence of the grain boundary (open circles). Figures 3 and 4 depict the bulk spin–spin (J_{ij}) and external field (H_n) interactions when these Morse potentials are transformed via Eqs. (4) and (5) and when the difference in chemical potential ($\mu^{\mathrm{Cu}} - \mu^{\mathrm{Bi}}$) is zero. For convenience, we define a normalized temperature based on the Morse well-depth parameters, $T^* = 2kT/(D^{\mathrm{Cu-Cu}} + D^{\mathrm{Bi-Bi}} - 2D^{\mathrm{Bi-Cu}})$. One unit of reduced temperature equals 2646 K.

The bulk layer–layer coupling $\langle J_{nn'} \rangle$ described by Eq. (8) is constant within the bulk and depends only on $|n - n'|$, the distance between the layers. Table III summarizes the terms contributing to $\langle J_{nn'} \rangle$ for a system with our geometry and range of potential, and Fig. 5 shows the form of the interlayer coupling $\langle J_{nn'} \rangle$, which extends in the bulk out to eight layers away. The relation of this system to a more familiar model with shorter-range interactions is worth noting. The anisotropic next-nearest-neighbor interactions (ANNNI) model[19] contains ferromagnetic interactions $J_0^{\mathrm{ANNNI}} > 0$ between adjacent sites within a layer, ferromagnetic interactions $J_1^{\mathrm{ANNNI}} > 0$ between adjacent sites in adjoining layers, and antiferromagnetic interactions $J_2^{\mathrm{ANNNI}} < 0$ between the closest sites two layers away. Mean-field solution of the ANNNI model, obtained by averaging within layers and characterized by positive $\langle J_{nn} \rangle$ and $\langle J_{nn\pm1} \rangle$ and negative $\langle J_{nn\pm2} \rangle$, displays a variety of modulated phases. In contrast, for our mean-field system, $\langle J_{nn} \rangle$ is

TABLE II. Morse parameters.

	D/eV	α/Å	β/Å^{-1}
Bi–Bi	0.405 495	1.108 479	3.557 974
Bi–Cu	0.152 710	1.211 087	3.190 156
Cu–Cu	0.355 941	1.334 628	2.822 338

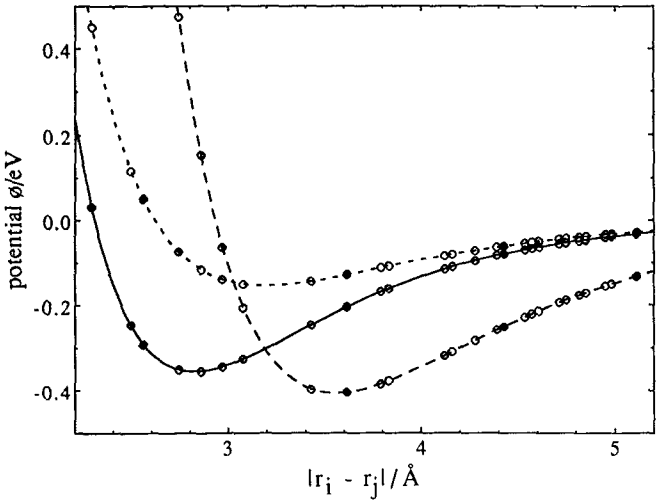

FIG. 2. Morse potentials ϕ vs distance [see Eq. (26)]. Bi–Bi interactions (long dashes), Cu–Cu (solid line), and Bi–Cu (short dashes). Table II gives the potential parameters. Filled circles correspond to lattice distances occurring in bulk copper, open circles to additional interactions introduced by the grain boundary.

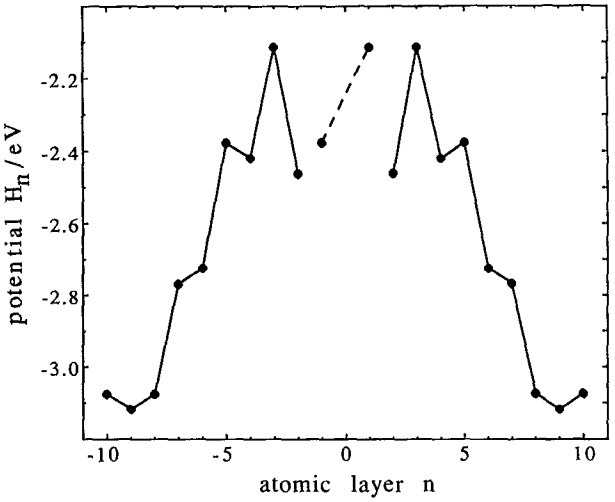

FIG. 4. Magnetic field H_n vs atomic layer. $H_n = H_{i_n} = 1/4\Sigma_j(\phi_{ij}^{\text{Cu-Cu}} - \phi_{ij}^{\text{Bi-Bi}})$, Eq. (5) with $\mu^{\text{Cu}} - \mu^{\text{Bi}} = 0$. Since there are two types of sites in the central layer, we distinguish between the magnetic fields which affect each sublattice. These two fields are shown connected by a dotted line.

positive, while $\langle J_{nn\pm1}\rangle$ is negative and $\langle J_{nn\pm2}\rangle$ is positive (Fig. 5). Also, the layer–layer interactions extend to $\langle J_{nn\pm8}\rangle$ and possess several terms of both signs. Despite these differences, we may expect modulated phases to appear at low temperature, since our system similarly contains competing interactions.

The Morse interactions are the only energetic terms put into the simulation—we make no *a priori* assumptions about an intrinsic energetic difference between the grain boundary region and the bulk region, such as an elastic strain energy. However, near the grain boundary, the atoms interact at internuclear separations not found in the bulk, and these chemical interactions are solely responsible for the segregation to the grain boundary in this model. In particular, the layer–layer interaction $\langle J_{nn'}\rangle$ and the magnetic field H_n become asymmetric near the grain boundary, since sites near the grain boundary interact with other sites at distances which do not occur in the bulk. Figure 4 shows how H_n varies as a function of distance from the grain boundary. Within an atomic layer, the sites are crystallographically equivalent, so H_n is constant in the x and y directions.

The central layer is treated differently, since two types of sites coexist there (see above). For clarity in Fig. 5 these are separated and placed on the " − 1" layer (for the original central sites) and on the " + 1" layer (for those sites arrowed in Fig. 1). The relative magnitudes of $(\phi_{ij}^{\text{Bi-Bi}} + \phi_{ij}^{\text{Cu-Cu}})$ and $\phi_{ij}^{\text{Bi-Cu}}$, as well as the chemical potentials μ^{Bi} and μ^{Cu}, determine the overall concentration ratio of Bi to Cu. Because of the relatively large value of $\phi^{\text{Bi-Bi}}$ at the nearest-neighbor distances, the magnetic field H_n is always negative and this inhibits the appearance of spin + 1, i.e., of

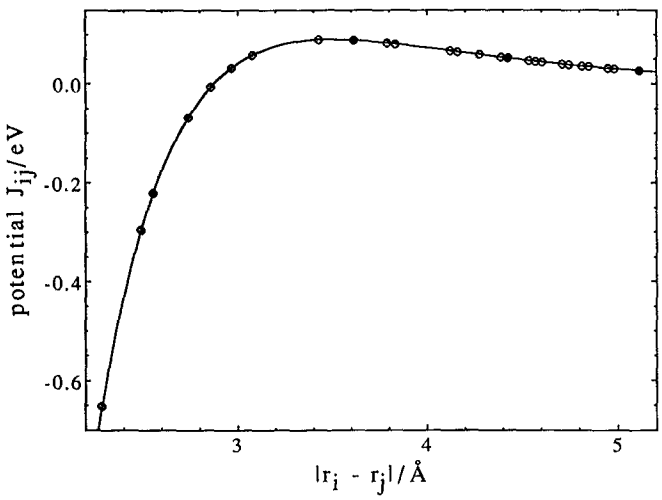

FIG. 3. Spin–spin coupling J_{ij} vs distance. $J_{ij} = 1/2[\phi_{ij}^{\text{Bi-Cu}} - 1/2(\phi_{ij}^{\text{Bi-Bi}} + \phi_{ij}^{\text{Cu-Cu}})]$, see Eq. (4). $J_{ij} > 0$ indicates ferromagnetism; $J_{ij} < 0$ indicates antiferromagnetism. Again, filled circles represent distances found in bulk copper, open circles to additional interactions introduced by the grain boundary.

TABLE III. Interlayer coupling $\langle J_{nn'}\rangle$ in the bulk.

$\lvert n - n'\rvert$	Spin–spin interactions[a]
0	$4J_2$
1	$2J_1 + 2J_3$
2	$J_1 + J_2 + 2J_3 + 2J_4$
3	$2J_1$
4	$J_1 + 2J_3 + J_4$
5	$4J_3$
6	$J_2 + 2J_4$
7	$2J_3$
8	J_4

[a] J_1 is the spin–spin coupling for the nearest-neighbor distance in the fcc crystal, J_2 is the coupling at the second-nearest-neighbor distance, etc., see Eq. (8).

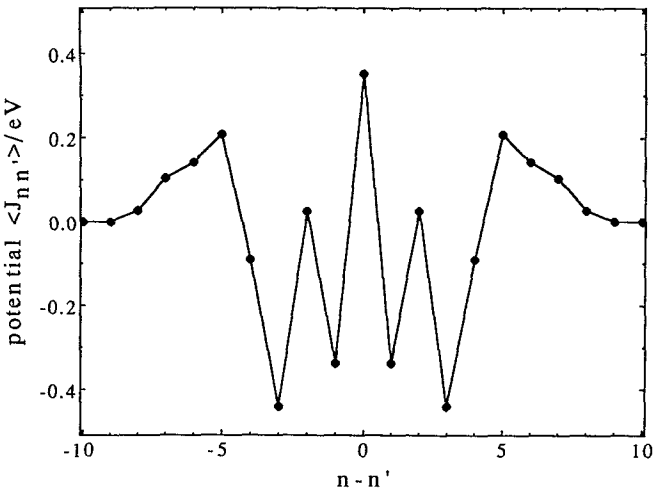

FIG. 5. Interlayer coupling vs distance. Bulk layer–layer coupling $\langle J_{nn'} \rangle = \Sigma_{j_n, j_{n'}} J_{i_n j_{n'}}$, where site i is in the nth layer and each site j is in the n'th layer [Eq. (8)]. The form of this coupling is symmetric in the bulk, but becomes asymmetric on approaching the grain boundary.

bismuth. This effect is least pronounced in the grain boundary region, which tends to enhance segregation, as pointed out in Sec. II A.

In this paper, we attempt to maintain a 15% bismuth concentration, corresponding to $\bar{A} = -0.7$. The solubility of bismuth in copper is on the order of 1% or less in the real physical system.[20] Our theoretical approach can in principle go to that or any other arbitrary concentration. However, Monte Carlo simulations can handle only systems with high enough concentrations to yield good statistics. 15% is a typical concentration for a Monte Carlo simulation of segregation,[9,17] so to facilitate future comparison with simulations we use a higher concentration than is experimentally attainable in copper/bismuth.

Table IV lists the d_{2p} discrete-difference coefficients, defined in Eq. (9), for our system with this particular geometry.

B. Results

1. Bulk system

Using the method described in the Sec. III, we determine the stable sinusoidal and cosinusoidal phases which give the lowest energy in the bulk over a wide temperature range. At $T^* = 12$, the paramagnetic ($\lambda = 1$) phase with magnetization $\bar{A} = -0.7$ (15% bismuth concentration) is the most stable phase. The amplitude for every other phase is zero. We then lower the temperature multiplicatively so that $T^* = 12(0.84)^n$, studying the system at a total of 20 discrete temperatures. Starting at $T^* = 3.541$, we observe that several ordered phases develop energies lower than the paramagnetic phase. Down to $T^* = 0.437$, the lowest investigated temperature, the pure sine and cosine concentration profiles which appear are the antiferromagnetic phase ($\lambda = 2$) and several ordered phases ($\lambda = 5$, 6, 7, and 8). We also solve for the zero-temperature phases by excluding the entropy term in G_{MF} and using the same procedures. We thereby determine that these ordered profiles are the only sine and cosine profiles at $T^* = 0$ with energies lower than the paramagnetic profile.

The magnetic field necessary to sustain three of these phases is shown in Fig. 6 as a function of temperature. As expected from Eq. (19), the magnetic field is linear for the paramagnetic ($q = 2\pi$) phase, but deviates from linearity for the ordered phases.

As explained above, these fields may correspond to profiles with different magnetizations and with different shapes than purely sinusoidal waves. We therefore perform local minimizations in the bulk at all 20 temperatures starting with the ($\lambda = 1$, 2, 5, 6, 7, and 8) sine and cosine phases at $\bar{A} = -0.7$, and with the previously determined magnetic field H.

A bulk local minimization which begins with a flat paramagnetic profile always ends with a flat profile. Therefore, the paramagnetic phase is always metastable, and we find that it is also the most stable phase from $T^* = 12$ to 4.216, inclusive. In fact for these higher temperatures, every mini-

TABLE IV. Lattice difference operator coefficients d_{2p}.

p	d_{2p}
0	$12J_1 + 8J_2 + 24J_3 + 12J_4$
1	$40J_1 + 40J_2 + 240J_3 + 160J_4$
2	$33J_1 + 106J_2 + 634J_3 + 568J_4$
3	$10J_1 + 112J_2 + 744J_3 + 904J_4$
4	$J_1 + 54J_2 + 462J_3 + 769J_4$
5	$12J_2 + 158J_3 + 376J_4$
6	$J_2 + 28J_3 + 106J_4$
7	$2J_3 + 16J_4$
8	J_4

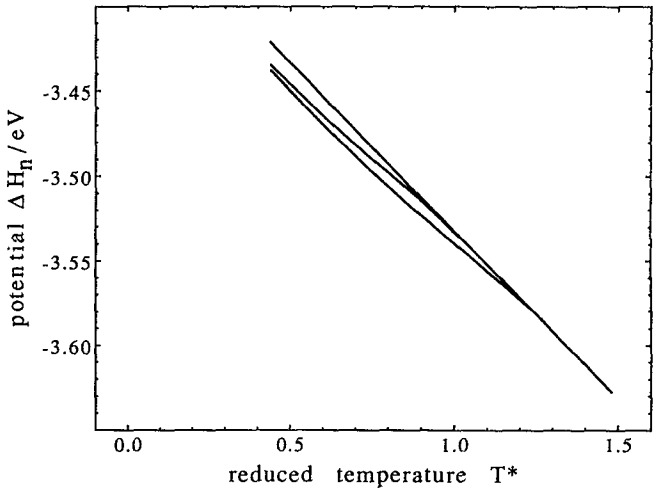

FIG. 6. Applied magnetic field vs temperature. Additional magnetic field $\Delta H_n [= 1/2(\mu^B - \mu^A)]$ necessary to sustain $\bar{A} = -0.7$ (15% Bi) for the ($\lambda = 1$) paramagnetic, ($\lambda = 6$) pure cosinusoidal, and ($\lambda = 7$) pure sinusoidal states. In order to focus on the difference between the paramagnetic and ordered fields at low temperatures, this figure depicts a smaller temperature range than actually studied. The magnetic field for the paramagnetic state is linear in temperature; the field for the ($\lambda = 7$) state lies directly below this, while that for the ($\lambda = 6$) state is the lowest at any given temperature.

mized sine and cosine profile results in a flat profile at 15% bismuth concentration.

A bulk local minimization which begins with an antiferromagnetic ($\lambda = 2$) profile also returns to a paramagnetic profile for all T^* down to $T^* = 3.541$. However, below that temperature, the antiferromagnetic phase persists upon local minimization. The energy of this antiferromagnetic phase, while lower than the paramagnetic phase, is higher than that of the most stable ordered phase, so we conclude that antiferromagnetic order is at best metastable over all investigated temperatures. Several other metastable phases also appear and disappear over various intermediate temperatures.

The first globally stable ordered phase appears at temperature $T^* = 3.541$. Thus, there is a phase transition from the paramagnetic phase to this ordered phase between $T^* = 4.216$ and 3.541. This profile [Fig. 7(a)] developed from minimization of the ($\lambda = 7$) sine concentration profile. At this temperature, its energy differs from the paramagnetic energy by $\sim 1\%$. This phase persists down to $T^* = 2.499$ and the energy difference between this and the paramagnetic phase increases at lower temperatures, while the amplitude of the concentration profile also increases.

At the next lower temperature $T^* = 2.099$, a square-wave profile derived from minimizing the ($\lambda = 6$) cosine profile now becomes the most stable phase. Again, the character of the ordered phase varies slightly with temperature. When the phase first appears [Fig. 7(b)], the peaks of the square waves are not completely flat. At the next examined temperature, $T^* = 1.763$, the concentration variation increases in amplitude, and from $T^* = 1.481$ down to the lowest temperature, the square waves are flat. In the absence of the entropy term in G_{MF}, local minimizations both on pure sine and cosine profiles and on the minimum free energy profiles obtained at nonzero T^*, indicate that this ($\lambda = 6$) square wave is the most stable profile at zero temperature as well.

In summary, from $T^* = 12$ to 4.216 inclusive, the bulk phase is uniform (paramagnetic) at 15% bismuth. From $T^* = 3.541$ to 2.499, an ordered ($\lambda = 7$) phase, depicted in Fig. 8(a), is the lowest energy phase. Finally, from $T^* = 2.099$ down to $T^* = 0$, the ($\lambda = 6$) square wave phase, shown in Fig. 8(b), is the most stable. Since the calculation can be performed at any temperature, one could determine the transition points for each of these phases by performing calculations at intermediate temperatures. However, our primary interest is the behavior of the grain-boundary region, so we characterize the bulk at 20 temperatures only. The Gibbs mean-field energies G_{MF} vs temperature for the paramagnetic and for these two ordered phases in a bulk system of 240 layers are shown in Fig. 8.

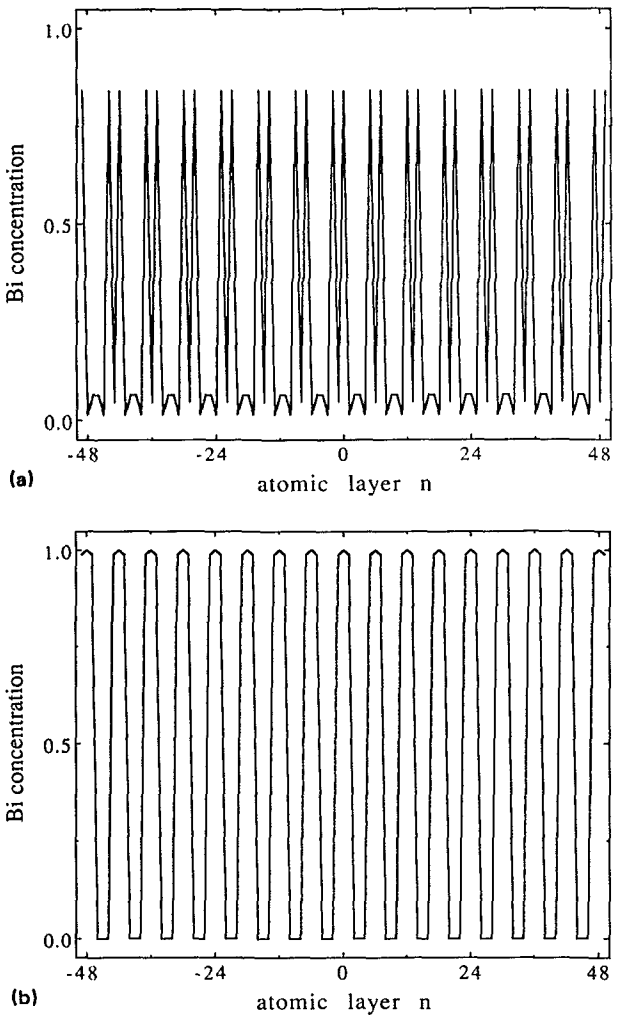

FIG. 7. Bulk concentration profiles. Each graph depicts the concentration of bismuth in [210] planes. In order to examine the detail of these profiles, only part of the 240-layer system is shown. One unit of reduced temperature T^* is 2646 K. (a) depicts a concentration profile at $T^* = 3.541$; this is also similar to profiles at $T^* = 2.975$ and 2.499. (b) depicts a concentration profile for $T^* = 1.763$ and resembles profiles from $T^* = 2.099$ to 0.437. Above $T^* = 3.541$, the bulk concentration profile is uniform at 15% bismuth ($\bar{A} = -0.7$). Below $T^* = 1.763$, the square wave depicted in (b) flattens out to three layers of 0% bismuth, alternating with three layers of 100% bismuth.

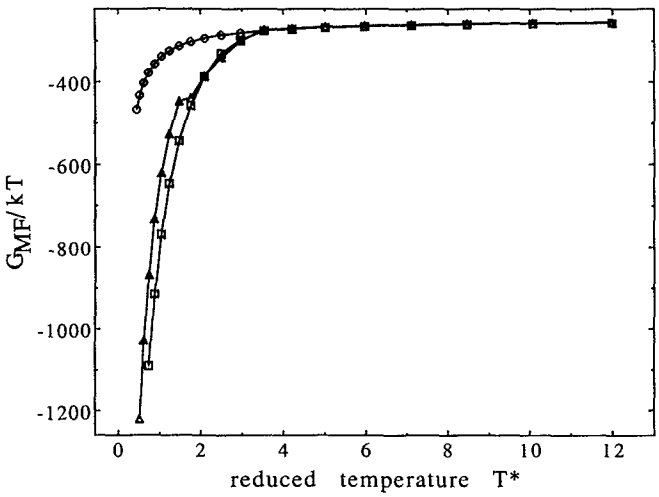

FIG. 8. G_{MF}/kT vs reduced temperature for $\lambda = 1$, 6, and 7. Mean-field Gibbs free energy, normalized by temperature, for the bulk phases after local minimization. Circles denote the energy of the paramagnetic state; triangles denote the energy of the ($\lambda = 7$) ordered state, and squares denote the energy of the ($\lambda = 6$) square wave state.

2. Grain boundary system

Since the paramagnetic phase is the most stable one at high temperature, we begin the local minimization of G_{MF} for the grain boundary system with a flat profile. Figures 9(a)–9(f) depict concentration profiles of the grain boundary systems; as for H_n in Fig. 4, the concentration in the central layer has been separated into two components representing the two types of atoms in the central layer.

The predominant feature is the appearance of bismuth

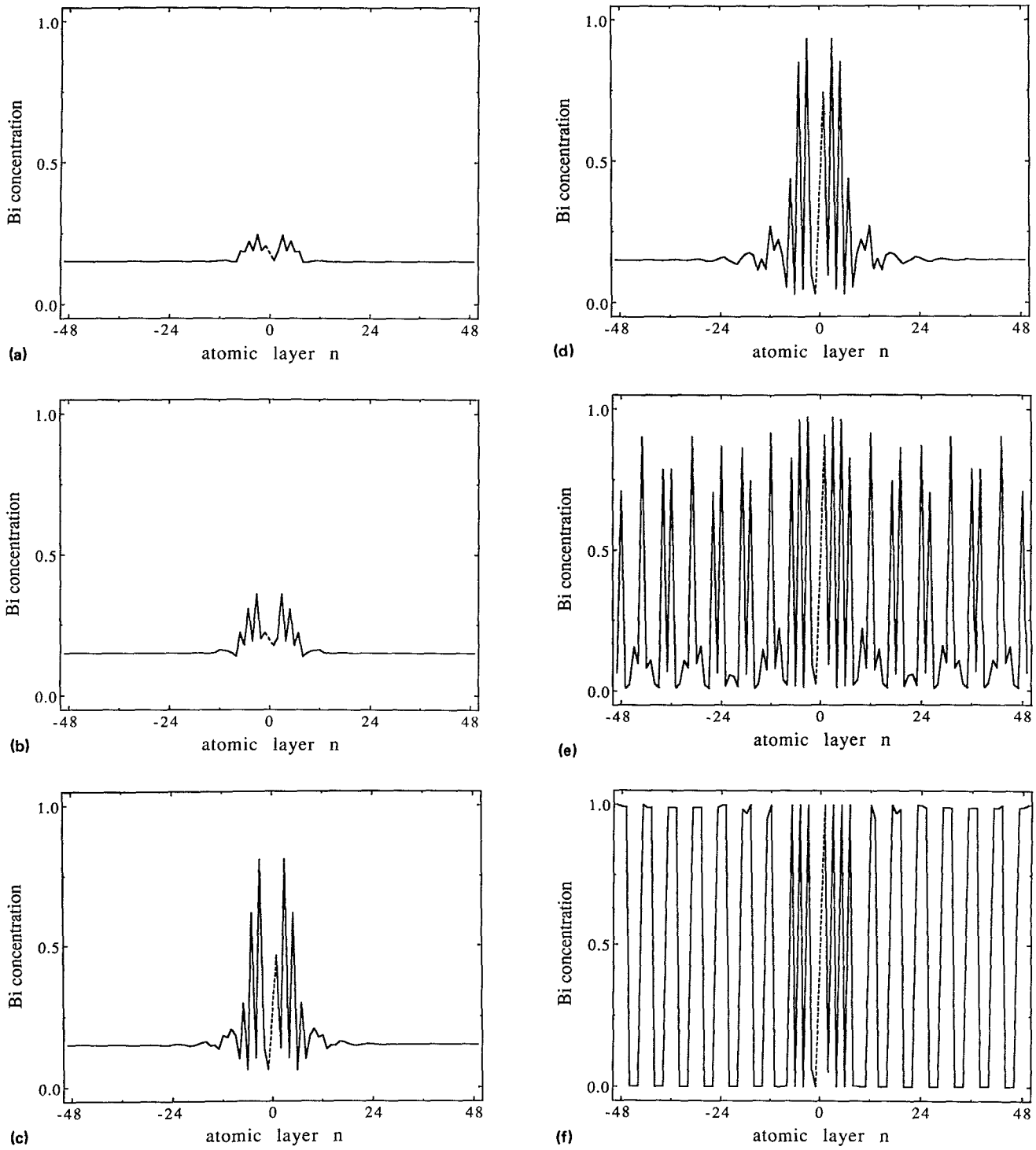

FIG. 9. Grain-boundary concentration profiles. These profiles were obtained by finding the local minimum in G_{MF} starting from a flat (paramagnetic) profile. As in Fig. 7, each graph depicts the concentration in [210] planes, which here are parallel to the grain boundary, and again only a detail of the full 240-layer system is shown. The concentration in the central layer, which consists of two sublattices, is separated out into layers -1 and $+1$, which are joined by a dotted line for clarity. (a)–(f) correspond to $T^* = 12.00$, 7.112, 5.019, 4.216, 3.541, and 1.763, respectively. See Sec. IV B 2 for a detailed discussion.

segregation at the grain boundary. The amount of bismuth at the boundary increases as we lower the temperature, consistent with the general phenomenon of segregation to solid–solid interfaces.[1,3] Furthermore, we can observe that the segregant is ordered near the boundary. Recent Monte Carlo[9,21] and experimental[21] studies appear to substantiate our observation that an oscillatory concentration profile can form near the grain boundary. Surface segregation has also recently been observed in a mean-field analysis of liquid interfaces,[12] where the presence of the interface was imposed by asymmetric spatial boundary conditions rather than by a discontinuity in the three-dimensional lattice geometry. The grain boundary introduces inhomogeneous spin interactions and this causes a considerably more complex behavior of the segregant in the system studied here.

In our system, layers in the boundary tend to be alternately rich and deficient in bismuth, and this antiferromagnetic type of ordering reflects the same variations found in the magnetic field (Fig. 5 and Secs. II A and IV A). The extent of segregation is apparent not only in the magnitude of these peaks, but also in their width. At the highest temperatures, large changes in the bismuth concentration occur only in the region where the magnetic field differs from the bulk value. The concentration outside this region does also vary, out to at least 20 layers from the central layer, but the variation is small ($<1\%$ bismuth) and is not apparent on the scale of these figures. Starting with $T^* = 7.112$, we begin to observe significant influence of the segregant on the concentration of the neighboring bulk region, visible in Fig. 9(b). This occurs now not because of variations in the field, but because of spin–spin coupling between the boundary layers and the nearby bulk layers.

As the temperature decreases, we observe increases in both the amount of segregation in the central layers, and in the width of the boundary [Figs. 9(c) and 9(d)]. At $T^* = 3.541$, we observe an even more striking result [Fig. 9(e)]. Starting from a *paramagnetic* profile, the profile which minimizes G_{MF} now results in an *ordered* profile. This occurs at the same temperature as when an ordered phase first becomes globally stable in the bulk [Sec. IV B 1 and Fig. 7(a)].

The spontaneous appearance of this phase in the grain boundary coinciding with the presence of the same ordered phase at the same temperature for the bulk system indicates that the grain boundary segregant can serve as a nucleus for the order–disorder transition. Recall that minimizing G_{MF} starting from the flat paramagnetic phase in a pure bulk system *never* yields any ordered states, even well below the transition temperatures; instead, the metastable paramagnetic phase persists. In fact, for the pure bulk system, at $T^* = 4.216$, no sinusoidal profile alone leads to the global minimum; it is necessary to input the globally stable profile from $T^* = 3.541$ in order to find the globally stable ordered profile at $T^* = 4.216$. However, in the grain boundary system, the high concentration of bismuth near the boundary influences the bulk by encouraging adjacent layers to order. As the temperature decreases further, the ordered state changes character. At $T^* = 2.099$ and below, the bulk portion of the concentration profile resembles the high-amplitude square waves found in the bulk system alone [compare Figs. 9(f) and 8(b)]. This is not a local phenomenon, as a system with 600 layers (342.8 Å) displays the same behavior. As with the onset of the ($\lambda = 7$) phase, this ($\lambda = 6$) square wave appears spontaneously at the transition temperature found in the bulk.

To reiterate, each of the profiles in Fig. 9 starts from a paramagnetic profile, but fluctuations in concentration due to the grain boundary disturb the flat profile and encourage the onset of the order–disorder transition. The energy minimization of a grain boundary system can also proceed starting with the bulk ordered profiles from Sec. IV B 1. The final grain boundary ordered profiles starting from these two different initial conditions have the same wavelength and amplitude. The small differences which appear in the bulk concentration profiles [between Figs. 8(a) and 9(e), and between Figs. 8(b) and 9(f)] are due partly to the grain boundary destroying the registry of the bulk phase. In the bulk calculations, the periodic boundary condition is set to an integral number of wavelengths, but in the presence of the grain boundary, the bulk phases may not align. In addition, the grain-boundary segregant influences the bulk layers nearest to the interface. Both of these effects introduce only a minor perturbation to the bulk phase structure.

In Figs. 9(e)–9(f), the presence of the bulk ordered phase makes it difficult to identify the grain boundary region, as the bulk interactions become relatively more influential than the inhomogeneous interactions found in the grain boundary. The concentration profile in Fig. 9(f) in particular shows how the bulk interactions have become important enough to eliminate the gross effects of the boundary. However, the profile is still antiferromagnetic in the boundary, while the ($\lambda = 6$) square wave dominates in the bulk.

In summary, over the temperature range $T^* = 12$–0.437, this method allows us to observe the details of boundary segregation, the influence of boundary segregation on the bulk substitutional order–disorder transition, and the dominance of that bulk ordered phase in the entire system at the lowest temperatures.

C. Discussion

As qualitatively predicted from segregation-isotherm models, the amount of bismuth segregation increases with lower temperature. However, unlike these basic models in which an *a priori* assumption must be made about the binding energy to place an impurity atom at the boundary, our energetics are based on existing bulk potentials and on the geometry of the lattice. When we transform these potentials to obtain the corresponding interactions in a spin Hamiltonian, we immediately see that the magnetic field near the boundary favors segregation, and that the shape of that magnetic field largely determines the shape of the concentration profile near the boundary.

Furthermore, because the bicrystal lattice is divided into atomic layers rather than into arbitrary bulk and grain-boundary regions, we observe how the segregant can form an ordered structure at the boundary. This result could never

have been predicted from the simpler isotherm models. In this particular copper/bismuth system, the concentration near the boundary is antiferromagnetic, with alternating layers rich and deficient with bismuth, while the bulk shows a longer wavelength modulation.

Since we use the finest possible division to examine the lattice in the z dimension, we also observe the artificiality of separating the bulk from a boundary region, because the width of boundary segregation changes with temperature. This occurs because long-range layer–layer couplings become more significant at lower temperatures, so the high concentration of bismuth near the boundary extends its influence to longer distances.

Finally, we observe that the boundary can influence the bulk to such an extent that segregation at the boundary can nucleate the order–disorder phase transition in the bulk. While we could not necessarily expect such long-range bulk ordering to occur in the physical copper/bismuth system because the solubility of bismuth in copper is extremely small,[20] this result is general and may occur in alloys where the solute can achieve high enough concentrations.

V. CONCLUSIONS

In this paper we have developed a general mean-field theory to predict the concentration profile in a crystalline lattice along one dimension. The theory, a natural extension to the atomic level of past segregation-isotherm models, is general for any set of pairwise interactions and does not require translation invariance. In spin terms, we are calculating the solution to a one-dimensional spin model with self-interactions, with inhomogeneous spin–spin interactions to eighth-nearest-neighbors in the bulk and tenth-nearest-neighbors near the grain boundary, and with an inhomogeneous magnetic field.

The shortcomings of this method stem from its mean-field approximation, which reduces the full three-dimensional bicrystal to one dimension. Since we assume that every site in a given layer has the same average concentration, the lateral distribution in the planes parallel to the boundary remains unknown. The exact nature of a phase transition in the three-dimensional system may also differ from the phase transition observed in this one-dimensional model. In addition, because we have solved this system in a grand-canonical manner, we depend on the magnetic field to control concentration and, as we have seen, an external field determined for a sinusoidal profile may not necessarily yield the desired concentration for the general profile at low temperature.

The theory does have several advantages over alternative theoretical methods. As mentioned before, its level of detail is much greater than the isotherm theories and is in fact the greatest possible for one-dimensional segregation profiles. Unlike computer simulations, which require a large number of sites to give good statistics at low concentrations, this method of solution is equally applicable to any solute concentration, as long as $dG_{\mathrm{MF}}/d\tau_n$ can be made small numerically. Furthermore, this method requires only a small amount of computational time compared to simulations. Finally, in contrast to mean-field studies of phase transitions in bulk systems, which often give only a general picture of the spin distribution at the transition, our theory provides a convenient way to obtain a detailed picture of the mean-field spin variable as a function of distance. Our theory also provides the only mean-field method to analyze a system with spatially inhomogeneous interactions of any finite range.

To summarize, this one-dimensional mean-field model complements current experimental work and theoretical insight on grain boundary segregation in the following ways. First, it predicts segregation as a function of temperature without assuming a binding energy beforehand. Second, it predicts the nature of the segregant on an atomic scale, including ordering and the broadening of the segregant distribution. Lastly, our theory illustrates that the ordered structure in the grain boundary can differ from the ordered structure in the bulk and, most significantly, indicates that the boundary segregant may nucleate substitutional order–disorder phase transitions in a binary alloy.

[1] *Interfacial Segregation*, edited by W. C. Johnson and J. M. Blakely (American Society for Metals, Metals Park, Ohio, 1977).

[2] J. B. Vander Sande, A. J. Garratt-Reed, Y.-M. Chiang, and T. Thorvaldsson, Ultramicrosc. **14**, 65 (1984); A. J. Garratt-Reed, Scanning Electron Microsc. **I**, 21 (1985).

[3] For a review on segregation isotherms, see, for example, *Adsorption on Metal Surfaces*, edited by J. Benard (Elsevier, New York, 1983); S. Hofmann, Scanning Electron Microsc. **III**, 1071 (1985).

[4] See, for example, A. P. Sutton and V. Vitek, Acta Metall. **30**, 2011 (1982); J. T. Wetzel and E. S. Machlin, Surf. Sci. **144**, 124 (1984).

[5] R. Herschitz and D. N. Seidman, Acta Metall. **35**, 1547 (1985).

[6] A. Brokman, Acta Metall. **35**, 307 (1987).

[7] M. Guttmann, Metall. Trans. A **8**, 1383 (1977); E. D. Hondros and M. P. Seah, *ibid.* **8**, 1363 (1977).

[8] For a collection of computer simulation techniques applied to solid–solid interfaces, see Surf. Sci. **144** (1984).

[9] W. L. Alba and K. B. Whaley, J. Chem. Phys. (submitted).

[10] P. H. Pumphrey, in *Grain Boundary Structure and Properties*, edited by G. A. Chadwick and D. A. Smith (Academic, San Francisco, 1976), pp. 139–200.

[11] B. Widom, J. Chem. Phys. **84**, 6943 (1986); K. A. Dawson, M. D. Lipkin, and B. Widom, *ibid.* **88**, 5149 (1988); K. A. Dawson, Phys. Rev. A **36**, 3383 (1987).

[12] K. A. Dawson, Phys. Rev. A **35**, 1766 (1987).

[13] S. Kirkpatrick, C. D. Gelatt, Jr., and M. P. Vecchi, Science **220**, 671 (1983).

[14] W. H. Press, B. P. Flannery, S. A. Teukolsky, and W. T. Vetterling, *Numerical Recipes* (Cambridge University, New York, 1986).

[15] L. A. Girifalco and V. G. Weizer, Phys. Rev. **114**, 687 (1959).

[16] A. Fraczkiewicz and M. Biscondi, J. Phys. (Paris) **46 C4**, 497 (1985).

[17] H. K. Chang, J. K. Lee, and D. F. Stein, in *Interatomic Potentials and Crystalline Defects*, edited by Jong K. Lee (Metallurgical Society of AIME, Warrendale, 1981), pp. 373–388. H. K. Chang, R. S. Weidman, and J. K. Lee, Surf. Sci. **144**, 224 (1984).

[18] A. Roy, U. Erb, and H. Gleiter, Acta Metall. **30**, 1847 (1982).

[19] M. E. Fisher and W. Selke, Philos. Trans. R. Soc. London **302**, 1 (1981); W. Selke and P. M. Duxbury, Z. Phys. B **57**, 49 (1984).

[20] D. J. Chakrabarti and D. E. Laughlin, Bull. Alloy Phase Diagrams **5**, 148, 203 (1984).

[21] S.-M. Kuo, A. Seki, Y. Oh, and D. N. Seidman, Phys. Rev. Lett. **65**, 199 (1990); S. M. Foiles and D. N. Seidman, MRS Bull. **15**, 51 (1990).